Acidity of edge surface sites of montmorillonite and kaolinite

Xiandong Liu[1, 2*], Xiancai Lu[1], Michiel Sprik[2], Jun Cheng[2], Evert Jan Meijer[3], Rucheng Wang[1]

[1]State Key Laboratory for Mineral Deposits Research, School of Earth Sciences and Engineering, Nanjing University, Nanjing 210093, P. R. China

[2]Department of Chemistry, University of Cambridge, Cambridge CB2 1EW, United Kingdom

[3] Van't Hoff Institute for Molecular Sciences and Amsterdam Center for Multiscale Modeling University of Amsterdam, Nieuwe Achtergracht 166, 1018 WV Amsterdam, The Netherlands

[*] Corresponding author: xiandongliu@gmail.com.

ABSTRACT Acid-base chemistry of clay minerals is central to their interfacial properties, but up to now a quantitative understanding on the surface acidity is still lacking. In this study, with first principles molecular dynamics (FPMD) based vertical energy gap technique, we calculate the acidity constants of surface groups on (010)-type edges of montmorillonite and kaolinite, which are representatives of 2:1 and 1:1-type clay minerals, respectively. It shows that ≡Si-OH and ≡Al-OH_2OH groups of kaolinite have p*K*as of 6.9 and 5.7 and those of montmorillonite have p*K*as of 7.0 and 8.3, respectively. For each mineral, the calculated p*K*as are consistent with the experimental ranges derived from fittings of titration curves, indicating that ≡Si-OH and ≡Al-OH_2OH groups are the major acidic sites responsible to pH-dependent experimental observations. The effect of Mg substitution in montmorillonite is investigated and it is found that Mg substitution increases the p*K*as of the neighboring ≡Si-OH and ≡Si-OH_2 groups by 2~3 p*K*a units. Furthermore, our calculation shows that the p*K*a of edge ≡Mg-$(OH_2)_2$ is as high as 13.2, indicating the protonated state dominates under common pH. Together with previous adsorption experiments, our derived acidity constants suggest that ≡Si-O- and ≡Al-$(OH)_2$ groups are the most probable edge sites for complexing heavy metal cations.

1. Introduction

Clay minerals, the ubiquitous components in soils and sediments, play important roles in numerous natural interfacial processes (Bergaya et al., 2006). Acid-base chemistry of clay minerals is essential to their interfacial properties, e.g. surface reactivity and colloidal property (Adams and McCabe, 2006; Lagaly, 2006; Lagaly et al., 2006). Clay minerals are widely applied in many industrial and engineering fields and the acid-base chemistry is also important for the practical applications, such as in catalysis industry and in environment engineering (Adams and McCabe, 2006; Lagaly, 2006; Lagaly et al., 2006). However, a quantitative understanding on their surface acidity is still lacking. For example, classical molecular simulations that are often used to study mineral water interfaces still require detailed protonation/deprotonation states of surface sites as an input because classical simulations cannot produce such information (Croteau et al., 2009; Rotenberg et al., 2007).

The crystal structures of layered silicates are formed by stacking structural layers along the *c*-axis. Generally, there are two major types of structural layers: 1:1-type and 2:1-type (Bergaya and Lagaly, 2006). In the former, the structural layer consists of stacked tetrahedral sheet (Si-O tetrahedrons) and octahedral sheet (mainly Al-O octahedrons) while in the latter, the structural layer is composed of octahedral sheet sandwiched by two tetrahedral sheets. Kaolinite and montmorillonite are the most two representative members of 1:1 and 2:1-type clay minerals, respectively. Due to the layered structures of clay minerals, there are two typical surface structures, namely, basal surfaces (i.e. interlayer surfaces) and edge surfaces (i.e. broken surfaces) (Schoonheydt and Johnston, 2006).

Montmorillonite has one type of basal surface (i.e. siloxane surface) and kaolinite has two: siloxane surface and hydroxyl surface. As extensive studies have been performed, the properties of the basal surfaces have been well documented (Schoonheydt and Johnston, 2006). Siloxane surfaces normally behave as adsorbing region for foreign molecules such as waters and cations, e.g. (Anderson et al., 2010; Liu and Lu, 2006; Vasconcelos et al., 2007). The OHs of hydroxyl basal surfaces of kaolinite can interact with foreign molecules via H-bonding (Tunega et al., 2002a) but they have minimal chemical reactivity and almost have no contribution to the acid-base chemistry of kaolinite (Brady et al., 1996; Schoonheydt and Johnston, 2006; Sposito, 1984). Therefore, the properties of clay basal surfaces are

52 considered to be pH-independent e.g. (Schoonheydt and Johnston, 2006; Vasconcelos et al., 2007). In
53 contrast, edge surfaces have more complicated structures and more subtle chemical properties, which
54 are generally pH-dependent. At these surfaces, many dangling bonds are present (e.g. ≡Al–O, ≡Si–O
55 and ≡Mg–O) and under ambient conditions, they are usually saturated by chemically adsorbed water
56 (Lagaly, 2006). The edge surface sites are normally amphoteric: as environmental pH increases, the
57 ligand gradually changes from $–OH_2$ to –O via –OH. This behavior leads to the pH-dependent
58 interfacial properties, such as complexing of heavy metal cations and organics (Lagaly, 2006).
59 Acid-base chemistry of edge surfaces is very difficult to study by using current experimental
60 techniques. While *in situ* techniques (e.g. spectroscopic methods) are still unable to provide quantitative
61 estimates, many macroscopic measurements such as titration have been carried out for phyllosilicates
62 including kaolinite and montmorillonite, e.g. see the recent studies of (Gu and Evans, 2008; Gu et al.,
63 2010) and references therein. In those studies, titration curves are fitted based on empirical adsorption
64 models and hence the proton binding constants can be derived. Although a large body of data have been
65 reported, the assignment of individual p*K*as to different surface groups is impossible. Therefore, the
66 accurate molecular level picture of acid chemistry of clay minerals is still unclear up to now, e.g. the
67 identities of active edge groups and their pristine p*K*as.
68 The study of interfacial structures and acidity was a challenge for first principles methods. By
69 combining static quantum mechanical calculations and bond valence theory, some researchers
70 (Bickmore et al., 2003; Bickmore et al., 2006; Churakov, 2006) derived acidity constants of edge groups
71 of pyrophillite (a neutral end member of 2:1 type phyllosilicates). The major shortcoming of such
72 approach is the oversimplification of solvent effects, which introduces errors to the interfacial
73 properties.
74 First principles molecular dynamics (FPMD) or density functional theory based molecular dynamics
75 (DFTMD) has been playing more and more important roles in research on mineral interface systems
76 (Boulet et al., 2006; Cygan et al., 2009; Marx and Hutter, 2009; Skelton et al., 2011; Suter et al., 2009;
77 Tunega et al., 2011). By combining electronic structure calculation and molecular dynamics, FPMD
78 treats the solute and solvent at the same theoretical level. FPMD has been used to investigate clay

systems, e.g. (Boek and Sprik, 2003; Churakov and Kosakowski, 2010; Larentzos et al., 2007; Liu et al., 2010; Liu et al., 2011; Ockwig et al., 2009; Suter et al., 2008; Tunega et al., 2004; Tunega et al., 2002b). In previous studies, FPMD simulations were employed to investigate the structures of edge-water interfaces for kaolinite and montmorillonite (Churakov, 2007; Liu et al., 2012a; Liu et al., 2012b). According to these studies, the microscopic interfacial structures are revealed and it is found that at around point of zero charge, stable edge sites include ≡Si-OH, ≡AlOH_2OH and ≡Mg-$(OH_2)_2$. FPMD based vertical energy gap method makes it feasible to calculate p*K*as of interfacial groups (Costanzo et al., 2011; Sulpizi and Sprik, 2008). This method has been successfully tested on many compounds including both molecules (Cheng et al., 2009; Costanzo et al., 2011; Mangold et al., 2011; Sulpizi and Sprik, 2008) and surface groups of minerals including rutile (Cheng and Sprik, 2010), quartz (Sulpizi et al., 2012) and pyrophillite (Tazi et al., 2012). Comparisons on acids and bases spanning 20 p*K*a units show that an accuracy of 2 p*K*a units can be achieved (Cheng et al., 2009; Costanzo et al., 2011; Sulpizi and Sprik, 2008; Sulpizi and Sprik, 2010).

In this study, we employ the vertical energy gap technique to calculate the acidity constants of (010)-type edge sites of montmorillonite and kaolinite. We collect experimentally derived acidity data in literature as extensively as we can. The comparison shows that the calculated p*K*as of ≡Si-OH and ≡Al-OH_2OH groups are overall in consistence with the experimental ranges of deprotonation constants and therefore, they are assigned to the major edge acidic sites. The effects of Mg substitution in montmorillonite are also studied. By integrating previous adsorption experiments, our derived acidity constants imply that the major edge sites for complexing heavy metal cations are ≡Si-O and ≡Al-$(OH)_2$.

2. Methodology

2.1. Models

The (010)-type interface models of kaolinite and montmorillonite (Fig. 1) are taken from our previous studies (Liu et al., 2012a; Liu et al., 2012b). Their chemical formulae are $Al_4Si_4O_{10}(OH)_8$ and $Li_{0.5}[Si_8][Al_{3.5}Mg_{0.5}]O_{20}(OH)_4$ respectively, which are derived from the reports of Bish (Bish, 1993) and Viani *et al*. (Viani et al., 2002). The edge surface model is cut from the unit cell and repeated along the *a* axis (x direction in Fig. 1) and each simulated model contains two unit cells. For the initial edge surface

106 models, the dangling ≡Si–O and ≡Al–O bonds are all saturated by protons. These edge models are
107 placed in 3D periodically repeated orthorhombic cells with the sizes of 10.34Å×30.0Å×7.39Å and
108 10.36Å×31Å×8.98Å for kaolinite and montmorillonite, respectively. These boxes have a solution
109 space of about 20 Å in the direction vertical to the edge surfaces (y direction in Fig. 1). The solution
110 regions of kaolinite and montmorillonite models contain 45 and 50 water molecules respectively. That
111 corresponds to a density of 0.98 g/ml, close to the density of bulk water at ambient conditions. Kaolinite
112 and montmorillonite systems contain totally 215 and 244 atoms, respectively.
113 Our previous study shows that for Mg cations at edge surface, only the 6-fold coordination is stable
114 i.e. the edge site is ≡Mg-$(OH_2)_2$ (Liu et al., 2012a). For Al at the edges of the two clay minerals, both the
115 6-fold and 5-fold coordinations are possible with the former being more stable, and therefore, only the
116 6-fold cases are investigated in this study. The investigated proton donating groups include ≡Si-OH,
117 OH_2 ligand of ≡Al-$OHOH_2$ and ≡Mg-$(OH_2)_2$ (for montmorillonite), and proton accepting sites are
118 oxygen of ≡Si-OH and OH of ≡Al-$OHOH_2$ (Liu et al., 2012a; Liu et al., 2012b). For proton accepting
119 sites, we calculate the p*K*as of their respective conjugate acids, that is, ≡Si-OH_2 and OH_2 of ≡Al-
120 OH_2OH_2. To reveal the effects of Mg substitution, two Si sites denoted as Si1 and Si2 are calculated:
121 Si2 connects with both Mg and Al while Si1 connects with Al only (Fig. 1).
122

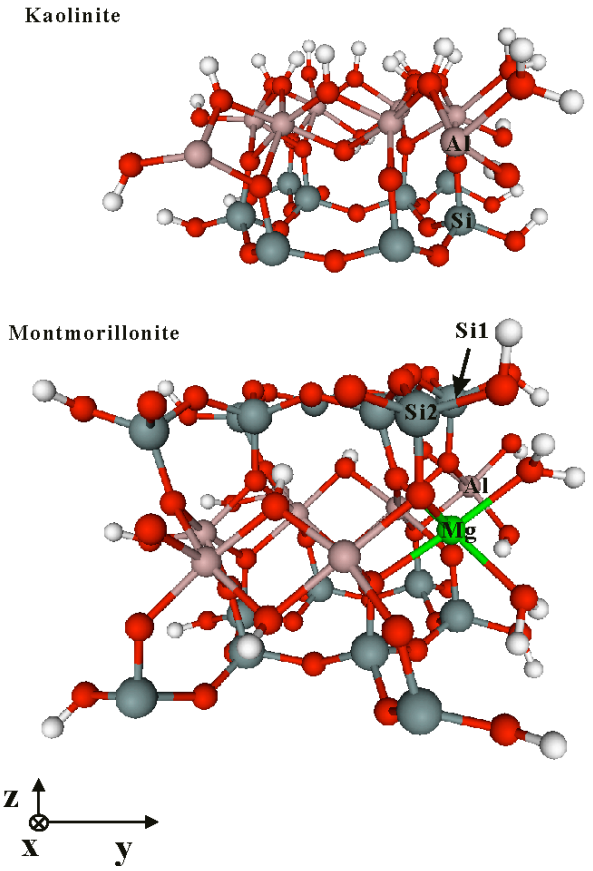

Figure 1. The used edge surface models of kaolinite and montmorillonite. The solution regions are on *y* direction. O = red, H = white, Si= grey Mg=green and Al = pink. In the montmorillonite model, Si2 connects with Mg via a bridge oxygen atom while Si1 connects with Al.

Our calculations indicate that ≡Si-OH and ≡Al-$(OH_2)_2$ groups have similar p*K*as and they are potential heavy metal cation complexing sites (see section 3.4). By taking Fe^{2+} as an example, we perform simulations of Fe^{2+} adsorbed on montmorillonite. For these simulations, the deprotonated group, i.e. ≡Si-O- or ≡Al-$(OH)_2$ serves as the complexation site. The protons are removed from the initial surface groups (i.e. ≡Si-OH or ≡Al-$(OH_2)_2$), and then Fe^{2+} cation is placed about 2.5 Å away from the O sites (this distance is taken from the Fe^{2+}-O_{water} RDF in aqueous solutions) (Herdman and Neilson, 1992).

2.2. First principles MD

The simulations are performed using CP2K/QUICKSTEP package (VandeVondele et al., 2005a). The electronic structures are calculated with density functional theory, which is implemented based on a

hybrid Gaussian plane wave (GPW) approach (Lippert et al., 1997). BLYP functional is used for the exchange-correlation (Becke, 1988; Lee et al., 1988). Goedecker-Teter-Hutter pseudopotentials (Goedecker et al., 1996) are employed to avoid calculations of core configurations. The plane wave kinetic energy cut off is set to be 280 Ry. For the simulations of Fe^{2+}-adsorbed systems, spin polarization calculation is performed with the high-spin state of Fe^{2+}.

Born-Oppenheimer molecular dynamics (BOMD) simulations are carried out with a wave function optimization tolerance of 1.0E−6 that allows a time step of 0.5 fs with reasonable energy conservation. The temperature is controlled at 330 K with the Nosé-Hoover chain thermostat. This temperature was used to avoid the glassy behaviour of BLYP liquid water as found at lower temperatures (VandeVondele et al., 2005b). For each system, an equilibration simulation is firstly performed for at least 2.0 ps and after that, the production run is carried out for 8.0 ps ~ 20.0 ps.

2.3. p*K*a calculations

The half-reaction scheme of the vertical energy gap method is employed to calculate p*K*as (Cheng et al., 2009; Costanzo et al., 2011). With this scheme, the proton of the acid (denoted as AH) is gradually transformed into a dummy (i.e. a classical particle with no charge). The free energy of the transformation for the acid is calculated with a thermodynamic integration technique:

$$\Delta_{dp}A_{AH} = \int_0^1 d\eta \left\langle \Delta_{dp}E_{AH} \right\rangle_{r\eta} \quad (1)$$

Here $\Delta_{dp}E$ is the vertical energy gap, defined as the difference of potential energies of the reactant state and the product state, which is calculated from the MD trajectories.

The averages of vertical energy gaps ($\Delta_{dp}E$) are calculated over the restrained mapping Hamiltonian:

$$\mathrm{H}_\eta = (1-\eta)\mathrm{H}_R + \eta\mathrm{H}_P \quad (2)$$

Where η is the coupling parameter which is increased from 0 (reactant) to 1 (product).

In practice, the Simpson rule is applied to evaluate the integral in Eq. 1, which requires the simulations at η=0, 0.5 and 1, respectively:

$$\Delta_{dp}A=\frac{1}{6}\left(\langle\Delta E\rangle_0+\langle\Delta E\rangle_1\right)+\frac{2}{3}\langle\Delta E\rangle_{0.5} \quad (3)$$

A restrained harmonic potential (V_r) is applied to keep the dummy atom in a location which resembles that of the acid proton of the reactant state:

$$V_r=\sum_{bonds}\frac{1}{2}k_d(d-d_0)^2+\sum_{angles}\frac{1}{2}k_\alpha(\alpha-\alpha_0)^2+\sum_{dihedrals}\frac{1}{2}k_\chi(\chi-\chi_0)^2 \quad (4)$$

This potential consists of the bonding, angle bending and torsions terms whose equilibrium values are d_0, α_0 and χ_0, respectively. The equilibrium values used for each surface group are obtained from the prior simulations without restraints and the restraining parameters have been selected according to the prescriptions of our previous studies (Cheng et al., 2009; Sulpizi and Sprik, 2008). Details of V_r are collected in Table 1.

The same procedure is applied to transform a proton of a hydronium located in the solution region into a dummy and the free energy of this transformation is denoted as $\int_0^1 d\eta\left\langle\Delta_{dp}E_{H_3O^+}\right\rangle_{r\eta}$.

The overall formula for pKa calculation reads:

$$2.30k_BTpK_a=\int_0^1 d\eta\left\langle\Delta_{dp}E_{AH}\right\rangle_{r\eta}-\int_0^1 d\eta\left\langle\Delta_{dp}E_{H_3O^+}\right\rangle_{r\eta}+k_BT\ln[c^0\Lambda_{H^+}^3] \quad (5)$$

c^0=1mol/L is the unit molar concentration and Λ_{H^+} is the thermal wavelength of proton (Costanzo et al., 2011). The third term $k_BT\ln[c^0\Lambda_{H^+}^3]$ accounts for the translational entropy generated by the acid dissociation and it is approximated by the chemical potential of a free proton at standard concentration. This term is equal to -0.19 eV or equivalently -3.2 pK units.

Table 1. The parameters used in the harmonic potentials (Eq. 4) restraining the dummy protons for kaolinite and montmorillonite. H_d means the dummy proton. n_d, n_α and n_χ stand for the numbers of the restrained bonds, angles and torsions, respectively. Equilibrium bond lengths (d_0) are in Bohr and equilibrium angles (α_0) and torsions (χ_0) are in radians. All the coupling constants are in a.u.

	Acids	n_d	d_0	k_d	n_α	α_0	k_α	n_χ	χ_0	k_χ
kaolinite	≡Si-OHH_d	2	1.92 1.92	1.0 1.0	2	1.87(H-O-H_d) 2.01(Si-O-H_d)	0.1 0.1	0	-	-
	≡Si-OH_d	1	1.90	0.1	1	2.06(Si-O-H_d)	0.1	1	0.52	0.1
	≡Al-OH_2OHH_d	1	1.92	0.1	2	1.85(H-O-H_d) 2.18(Al-O-H_d)	0.1	0	-	-
	≡Al-$OHOHH_d$	1	1.90	0.1	2	1.85(H-O-H_d) 2.08 (Al-O-H_d)	0.1	0	-	-
	$H_2H_dO^+$	3	1.89	1.0	2	1.94 (H-O-H_d) 1.94 (H-O-H_d)	0.1	0	-	-
montmorillonite	≡Si1-OHH_d	2	1.92 1.92	1.0 1.0	2	1.83 (H-O-H_d) 2.0 (Si-O-H_d)	0.1 0.1	0	-	-
	≡Si1-OH_d	1	1.90	0.1	1	2.04 (Si-O-H_d)	0.1	1	1.21	0.1
	≡Si2-OHH_d	2	1.92 1.92	1.0 1.0	2	2.06 (H-O-H_d) 2.27 (Si-O-H_d)	0.1 0.1	0	-	-
	≡Si2-OH_d	1	1.90	0.1	1	2.09 (Si-O-H_d)	0.1	1	0.87	0.1
	≡Al-OH_2OHH_d	1	1.92	0.1	2	1.83 (H-O-H_d) 2.18 (Al-O-H_d)	0.1	0	-	-
	≡Al-$OHOHH_d$	1	1.90	0.1	2	1.91 (H-O-H_d) 2.02 (Al-O-H_d)	0.1	0	-	-
	≡Mg-H_2OHH_d	1	1.92	0.1	2	1.87 (H-O-H_d) 2.09 (Mg-O-H_d)	0.1	0	-	-
	$H_2H_dO^+$	3	1.89 1.89 1.89	1.0	2	1.94 (H-O-H_d) 1.94 (H-O-H_d)	0.1	0	-	-

3. Results and discussion

3.1. Kaolinite

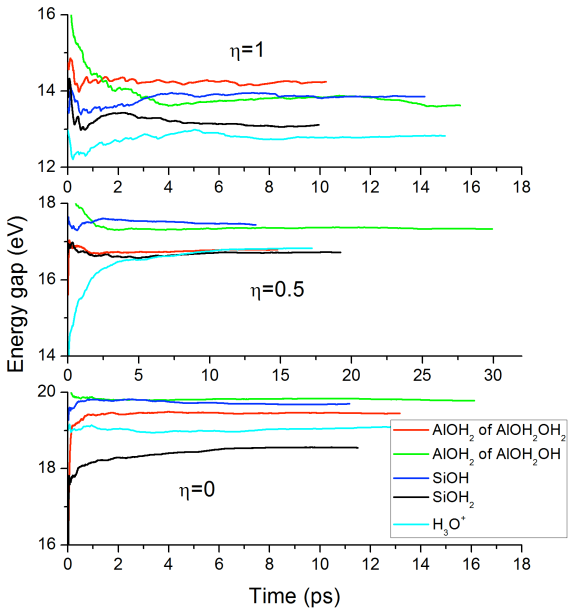

Figure 2. Accumulating averages of vertical energy gaps for groups on kaolinite (010) surface.

Table 2 Free energies (in eV) and p*K*as of edge surface groups of kaolinite.

Groups	≡Si-OH /≡Si-OH_2	≡Al-OH_2OH /≡Al-OH_2OH_2	H_3O^+
ΔA	17.23±0.03 /16.42±0.01	17.16±0.01 /16.83±0.02	16.63±0.03
p*K*a	6.9±1.0 /-6.7±0.7	5.7±0.7 /0.2±0.8	-

The error in p*K*a is calculated as the sum of the error in the deprotonation free energy of each surface group and of the error in the deprotonation free energy of the hydronium. Statistical errors in deprotonation free energies are calculated as the semi-difference between the values using the first half or the second half of the trajectory only.

Table 3 Acidity constants of kaolinite derived from experiments. □SOH denotes proton active sites.

Surface groups	≡SOH_2^+→≡SOH+H^+	□SOH□□SO-+H^+
(Schindler et al., 1987)	-4.37	9.18
(Brady et al., 1996)	2.33 (≡$AlOH_2^+$)	5.28 (≡AlOH) 8.23 (≡SiOH)
(Angove et al., 1998)	-3.24	7.15

(Ikhsan et al., 1999)	-3.96	7.24
(Srivastava et al., 2005)	-3.81	6.16
(Gu and Evans, 2008)	-4.63	7.54

193

194 Figure 2 illustrates the accumulating averages of vertical energy gaps for sites on kaolinite (010)
195 surface and Table 2 lists the derived free energy values and p*K*as. The statistical error (Table 2) in each
196 p*K*a is obtained as the sum of the error in deprotonation free energy of each surface site and of the error
197 in deprotonation calculation of the hydronium. The error in each deprotonation free energy is calculated
198 as the semi-difference between the values using the first half or the second half of the trajectory. It can
199 be seen that these errors are in 0.7~1.0 p*K*a units and such errors are of the same order as in our
200 previous study of the acidity of quartz (Sulpizi et al., 2012).

201 Table 3 collects the experimentally fitted acidity constants in literature, where one can see that most
202 studies employed 1-site model except the study of Brady et al (Brady et al., 1996). The calculated p*K*as
203 of ≡Si-OH and OH_2 of ≡Al-OH_2OH are very close: 6.9 vs 5.7. These values coincide with the
204 experimentally fitted acidity range based on 1-site model: 5.28~9.18 (see Table 3). This agreement
205 indicates that ≡Si-OH and the OH_2 of ≡Al-OH_2OH correspond to the proton-donating sites detected in
206 titration measurements.

207 ≡Si-OH_2 has a p*K*a of -6.7, about 2 p*K*a units smaller than the lower limit of the experimental range of
208 -4.63~-3.24 (Table 3). The p*K*a of ≡Al-(OH_2) is predicted to be 0.2, which does not have a
209 correspondence in the experimental results. Similar discrepancy has been found in the case of
210 montmorillonite (see section 3.2) and these are discussed for the two minerals in section 3.3.

211 **3.2. Montmorillonite**

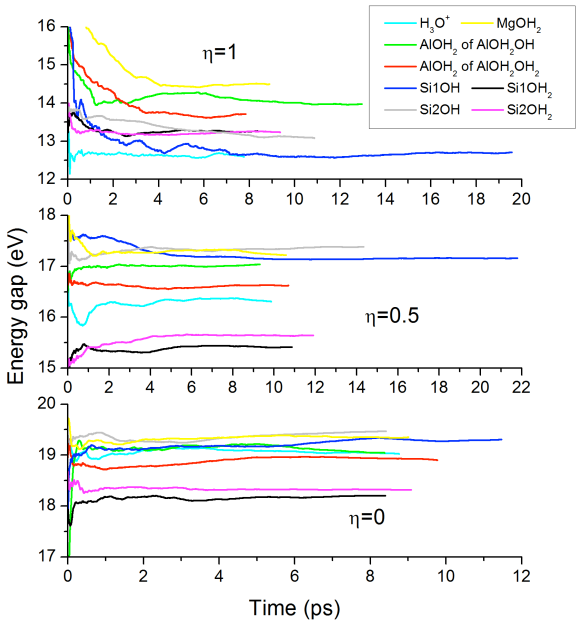

212

213 Figure 3. Accumulating averages of vertical energy gaps for groups of montmorillonite (010) surface.

214 Table 4 Free energies (in eV) and p*K*as of edge surface groups of montmorillonite.

Groups	≡Si1-OH /≡Si1-OH_2	≡Si2-OH /≡Si2-OH_2	≡Al-OH_2OH /≡Al-OH_2OH_2	≡Mg-OH_2OH_2	H_3O^+
ΔA	16.77±0.02 /15.50±0.01	16.98±0.01 /15.70±0.02	16.83±0.04 /16.52±0.01	17.12±0.01	16.15±0.02
p*K*a	7.0±0.7 /-14.3±0.5	10.8±0.5 /-10.9±0.7	8.3±1.0 /3.1±0.5	13.2±0.5	-

215 The error in p*K*a is calculated as the sum of the error in the deprotonation free energy of each surface group and of the
216 error in the deprotonation free energy of the hydronium. Statistical errors in deprotonation free energies are calculated
217 as the semi-difference between the values using the first half or the second half of the trajectory only.

218 Table 5. Acidity constants of montmorrillonite derived from experiments. ☐SOH stands for proton

219 active surface sites.

	Clay source	$\equiv SOH_2^+ \rightarrow \equiv SOH + H^+$	$\equiv SOH \rightarrow \equiv SO^- + H^+$
(Schindler et al., 1987)	Wyoming	-8.16 ($\equiv S_1OH_2$)	8.71 ($\equiv S_1OH$) 5.77 ($\equiv S_2OH$)
(Charlet et al., 1993)	SWy-1	-4.80	6.96
(Wanner et al., 1994)	-	-5.4	6.7
(Zachara and Smith, 1994)	Wyoming	0.95 ($\equiv SiOH_2$)	6.65 ($\equiv SiOH$)

		-5.78 (≡$AlOH_2$)	11.5 (≡AlOH)
(Bradbury and Baeyens, 1997)	SWy-1	-6.0 (≡S_1OH_2) -4.5 (≡S_2OH_2)	10.5 (≡S_1OH) 7.9 (≡S_2OH)
(Avena and De Pauli, 1998)	Argentinean	-2.97	6.1
(Kraepiel et al., 1999)	-	-5.6 (≡S_1OH_2) -4.5 (≡S_2OH_2)	8.7 (≡S_1OH) 5.5 (≡S_2OH)
(Ikhsan et al., 1999)	Gonzales, Texas	-3.9	7.2
(Ikhsan et al., 1999)	SWy-2	-5.0	7.2
(Barbier et al., 2000)	SWy-2	-4.38	5.26
(Tombacz et al., 2004; Tombacz and Szekeres, 2004)	SWy-2	-5.1	7.9
(Tournassat et al., 2004)	-	-10.5 (≡$AlOH_2$)	8.2 (≡SiOH) 7.2 (≡AlSiOH) 4.8 (≡Al_2OH)
(Tertre et al., 2006)	MX-80	-5.1 (≡$AlOH_2$)	8.5 (≡AlOH) 7.9 (≡SiOH)
(Gu et al., 2010)	Wyoming	-6.04	6.63
(Marcussen et al., 2009)	SWy-1	-5.1	8.5

Figure 3 shows the accumulating averages of vertical energy gaps for montmorillonite-(010) sites. Table 4 lists the calculated free energies and p*K*as, where one can see that similar to the results of kaolinite (Table 2), the statistical errors are within 1.0 p*K*a unit. Due to the much more complex compositions, montmorillonite has more complicated acid chemistry than kaolinite. As shown in Table 5, previous experimental works on montmorillonite present obviously bigger variations than that of kaolinite: from 4.8 to 11.5 for ≡SOH sites and from -10.5 to 0.95 for ≡SOH_2 sites. Even with the similar samples, different acidity constants are obtained by different groups, e.g. for SWy-2 clay, Barbier et al (2000) derived 5.26 for ≡SOH while Tombacz et al. (2004) reported 7.9.

Just as the case of kaolinite, there are more 1-site based fitting studies than multi-site works for montmorillonite. For the 1-site based studies, the p*K*a range for the deprotonation constants of ≡S-OH site is 5.26~8.5. For the multi-site based works, the p*K*a range is very similar: 4.8~8.71 given that the two high values, 10.5 (Bradbury and Baeyens, 1997) and 11.5 (Zachara and Smith, 1994), are not included.

From the derived data set in Table 4, one can see that the p*K*as of ≡Si1-OH and ≡Al-OH_2 of ≡Al-OH_2OH, i.e. 7.0 and 8.3, are in good consistence with the experimental range. These two values also agree with the p*K*as of their counterpart edge sites (6.8 and 7.6 for ≡Si-OH and ≡Al-OH_2OH respectively) reported in a recent study (Tazi et al., 2012), where the neutral clay framework (i.e. without substitution) is investigated. In contrast, ≡Si2-OH site where Si atom connects with Mg atom via one bridge oxygen (Fig. 1) has a significantly higher p*K*a, 10.8. This indicates that the effect of isomorphic substitution on the acidity of edge site is relatively short ranged.

≡Mg-$(OH_2)_2$ has a p*K*a of 13.2, only 2 p*K*a units lower than p*K*w, which agrees with the fact that Mg^{2+} is a poor hydrolyzing cation (p*K*a=11.4) (Westermann et al., 1986). This p*K*a indicates that under common pH range, all of ≡Mg-$(OH_2)_2$ groups are protonated and do not take part in common acid titration processes. Table 4 shows that Mg substitution increases the p*K*as of adjacent ≡Si-OH and ≡Si-OH_2 groups: ≡Si2-OH and ≡Si2-OH_2 have p*K*a values of 10.8 and -10.9, which are over 3 p*K*a units higher than those of Si1 site. The p*K*a of ≡Si2-OH is close to the values of the weak sites of p*K*as, 10.5 and 11.5 as mentioned above (Zachara and Smith, 1994; Bradbury and Baeyens, 1997). This implies that the high p*K*a values may originate from Mg substitutions, which are ubiquitous in montmorillonite.

The p*K*a of ≡Al-$(OH_2)_2$ site is predicted to be 3.1 (Table 4), which may correspond to the low p*K*a constants in Table 5, i.e. 4.8 (Tournassat et al., 2004), 5.26 (Barbier et al., 2000) and 5.5 (Kraepiel et al., 1999).

OH_2 ligands of ≡Al-$OHOH_2$ and ≡Al-$(OH_2)_2$ have p*K*a values of 8 and 3.1, respectively (Table 4) and these values are 2~3 p*K*a units higher than those of ≡Al-$(OH_2)_2$ site in kaolinite. For this group, the difference between the two minerals is that in kaolinite, the edge Al atom connects with two OHs on the basal surface whereas in montmorillonite, the Al atom connects with two bridge oxygen bonding with Si

256 in tetrahedral layers (see Fig. 4). In a view of electronegativity, bridge oxygen is more negative than the
257 oxygen of the surface OHs in kaolinite: Mulliken population analyses show that the bridge O has an
258 average partial charge of -1.15*e* while the OH oxygen atom has -1.05*e* (Cygan et al., 2004). This
259 eventually leads to that the OH_2 ligand in montmorillonite is less acidic than that OH_2 in kaolinite.

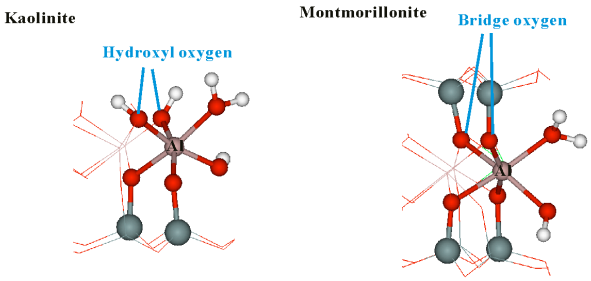

260

261 Figure 4. Models of (010)-type edge surfaces highlighting the Al-O octahedrons. O = red, H = white,
262 Si= grey and Al = cyan.

263 **3.3. Implication for titration experiments**

264 It was thought that the comparison between ab initio predicted and titration derived acidity constants
265 is not possible and therefore previous studies made comparisons with results from bond valence theory
266 rather than experiments (Bickmore et al., 2003; Tazi et al., 2012). However, as discussed above, one
267 finds good agreement between the p*K*as of ≡Si-OH and ≡Al-$OHOH_2$ sites and experimental values. For
268 each clay mineral, the two acidic sites (i.e. ≡Si-OH and ≡Al-$OHOH_2$) have very close p*K*a values: 6.9 vs
269 5.7 for kaolinite and 7.0 vs 8.3 for montmorillonite, that is, the difference is within only 1.3 p*K*a units.
270 Although montmorillonites have considerable Mg substitutions, the calculated p*K*a for ≡Mg-$(OH_2)_2$,
271 13.2, is significantly beyond the common experimental pH range (3~9) and therefore these groups do
272 not contribute to proton dissociation. These data explain why the 1-site based approach generally works
273 well in numerical fitting of titration curves for both minerals. On the other hand, one can easily
274 understand that due to the similar deprotonation constants, they cannot be distinguished through the
275 titration curve fitting approach.

276 In contrast, for their conjugate acids (i.e. ≡Si-OH_2 and ≡Al-$(OH_2)_2$), it is not easy to make direct
277 comparison with experiments. For montmorillonite, the calculated values of ≡Si1-OH_2/≡Si2-OH_2 and

278 ≡Al-$(OH_2)_2$ are -14.3/-10.9 and 3.1, respectively and for kaolinite, the results are -6.7 and 0.2
279 respectively. These ≡Si-OH_2 p*K*as are in line with the strong acid characteristics of ≡Si-OH_2 site (Sulpizi
280 et al., 2012). One can see that the p*K*as of these conjugate acids envelope the fitted acidity ranges of
281 strong acid sites (i.e. ≡Si-OH_2 sites: -4.63~2.33 for kaolinite in Table 3 and -10.5~0.95 for
282 montmorillonite in Table 5). One important reason is that they have relatively bigger differences in p*K*as
283 and therefore, when one tries to fit the titration data with 1-site model, error is inevitable to be included.
284 Another origin for this discrepancy is the lack of titration data at the low pH end. Almost all titration
285 measurements are performed over the common pH, i.e. 3~9 and the limited pH range makes it hard to
286 investigate the sites of low p*K*as, because those sites only show significant proton binding in very low
287 pH range. Unfortunately, one serious problem with low pH is the acid induced mineral dissolution,
288 which is very hard to circumvent in practice and therefore, the experimental data in low pH range are in
289 bad need.

290 **3.4. Implication for heavy metal cations complexing**

291 Adsorption of heavy metal cations on clay minerals is an important chemical process controlling their
292 migration and bioavailability in soils and aquifers. On the other hand, clays are applied as
293 environmental materials to fix toxic heavy metals. Therefore, this topic has attracted significant
294 attentions (Churchman et al., 2006). Numerous experiments have shown that adsorption of heavy metal
295 cations on clay minerals consists of two stages as pH increases: cation exchange and edge complexing
296 steps, e.g. ((Gu and Evans, 2008; Gu et al., 2010) and references therein). The first step happens
297 between foreign cations and interlayer exchangeable cations, which is pH independent. The second step
298 happens on edge surfaces and it is obviously pH dependent. It is generally accepted that the pH for the
299 start of edge complexing step is approximately 5~7. For example, for Zn^{2+} adsorption on
300 montmorillonite and kaolinite, Ikhsan obtained 7.0 for the starting pH for edge complexing stage
301 (Ikhsan et al., 2005); Schultz and Grundl show that the starting pH for Fe^{2+} complexation on
302 montmorillonite is 6.75 (Schultz and Grundl, 2004); Gu et al obtained about 6.0 for Ni^{2+}, Cd^{2+}, Cu^{2+},

303 Zn^{2+} on montmorillonite (Gu et al., 2010) and around 5.0 for kaolinite (Gu and Evans, 2008). Although
304 many experimental works have been carried out, the accurate adsorption mechanism is still unclear.
305 Our calculated acidity constants (Table 2 and Table 4) show that as pH increases to be above 5.0, the
306 deprotonated forms of ≡Si-OH and ≡Al-$OHOH_2$ gradually become predominant. Therefore, the edge
307 sites (i.e. ≡Si-O and ≡Al-$(OH)_2$) become potential sites for heavy metal cations to form inner-sphere
308 complexes. By taking Fe^{2+} as an example, the simulations show that monodentate and bidentate Fe^{2+}-
309 complexes form on ≡Si-O and ≡Al-$(OH)_2$ sites respectively, i.e. □Si-O-$Fe(H_2O)_5$ and □Al-$(OH)_2$-
310 $Fe(H_2O)_4$ (Fig. 5). In the simulation periods of over 20 ps, these complexes hold stable. For □Si-O-
311 $Fe(H_2O)_5$, the average Fe^{2+}-O bond length is about 2.02 Å, which is consistent with our previous study
312 of ≡Si-O-Fe^{2+} complex at the edge of neutral clay frameworks (Liu et al., 2012c). For □Al-$(OH)_2$-
313 $Fe(H_2O)_4$ complex, the two Fe^{2+}-O lengths are around 2.08 Å but the two Al-O bonds should strengthen
314 the complexing.
315 There are still many open questions that need to be addressed to understand acid-base chemistry of
316 clay minerals at a molecular level, and such a fundamental understanding is most likely to be achieved
317 through the synergy between experiments, modeling and atomistic simulations. By combining FPMD
318 derived p*K*as and the modeling approach (Bourg et al., 2007), the titration curve could be reproduced
319 for clay minerals and can be compared with the experimental data. On the other hand, FPMD
320 simulations are able to provide precise structural data which can be used for fitting EXAFS (Extended
321 X-ray absorption fine structure) measurements and furthermore, FPMD based free-energy calculation
322 methods (e.g. metadynamics (Laio and Parrinello, 2002), constrained MD (Sprik, 2000; Sprik and
323 Ciccotti, 1998)) can give reasonable estimates of the free-energy surfaces of complexes (Churakov and
324 Daehn, 2012), e.g. adsorption free energies of complexes on silanol and aluminol sites and thus their
325 relative populations. This will be addressed in our future research.
326

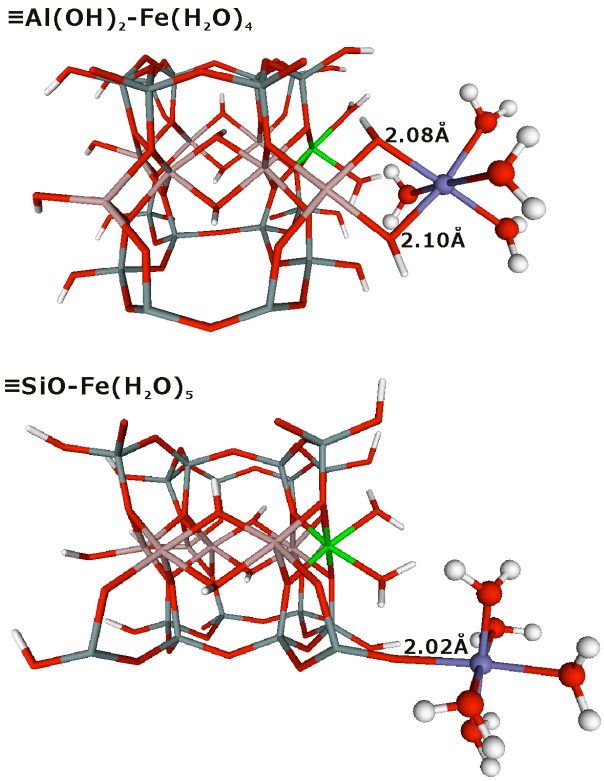

Figure 5. Fe^{2+}-complexes adsorbed on (010) edge surface of montmorillonite.

4. Summary

By using the recently developed FPMD based vertical energy gap method, we derive the acidity constants of (010)-type edge surfaces of montmorillonite and kaolinite. It shows that ≡Si-OH and ≡Al-OH_2OH groups of kaolinite have p*K*as of 6.9 and 5.7 and those sites of montmorillonite have p*K*as of 7.0 and 8.3, respectively. For each mineral, the calculated acidity constants coincide with the acidity ranges derived from titration curve fitting. Therefore, the edge acidic sites responsible to pH dependent phenomena are assigned to these two surface groups. Because for both minerals, ≡Si-OH and ≡Al-OH_2OH sites have very close p*K*as, they are almost indistinguishable in titration experiments. For the ubiquitous Mg substitution in montmorillonite, it is found that ≡Mg-$(OH_2)_2$ is the usual form under common pH ranges due to its high p*K*a of 13.2 and Mg substitution increases the p*K*as of the neighboring ≡Si-OH/≡Si-OH_2 groups by 2~3 p*K*a units. Together with previous adsorption experiments, our derived acidity constants imply that the deprotonated forms of ≡Si-OH and ≡Al-OH_2OH (i.e. ≡Si-O- and ≡Al-$(OH)_2$ groups) are the most probable sites for complexing heavy metal cations.

Acknowledgment We thank Prof. Marc Norman, Prof. James Rustad and three anonymous reviewers for the comments. We acknowledge National Science Foundation of China (Nos. 41002013, 40973029, 41273074 and 41222015), Natural Science Foundation of Jiangsu Province (BK2010008), Newton International Fellow Program and the financial support from the State Key Laboratory for Mineral Deposits Research. We are grateful to the High Performance Computing Center of Nanjing University for using the IBM Blade cluster system.

References

Adams J.M. and McCabe R.W. 2006 Clay minerals as catalysts. In: Bergaya, F., Theng, B.G.K., Lagaly, G. (Eds.), Handbook of Clay Science. Elsevier, Amsterdam, pp. 541-582.

Anderson R.L., Ratcliffe I., Greenwell H.C., Williams P.A., Cliffe S. and Coveney P.V. (2010) Clay swelling - A challenge in the oilfield. *Earth-Science Reviews* **98**: 201-216.

Angove M.J., Johnson B.B. and Wells J.D. (1998) The influence of temperature on the adsorption of cadmium(II) and cobalt(II) on kaolinite. *Journal of Colloid and Interface Science* **204**: 93-103.

Avena M.J. and De Pauli C.P. (1998) Proton adsorption and electrokinetics of an Argentinean montmorillonite. *Journal of Colloid and Interface Science* **202**: 195-204.

Barbier F., Duc G. and Petit-Ramel M. (2000) Adsorption of lead and cadmium ions from aqueous solution to the montmorillonite/water interface. *Colloids and Surfaces a-Physicochemical and Engineering Aspects* **166**: 153-159.

Becke A.D. (1988) Density-functional exchange-energy approximation with correct asymptotic-behavior. *Physical Review A* **38**: 3098-3100.

Bergaya F. and Lagaly G. 2006 General Introduction: Clays, Clay Minerals, and Clay Science. In: Bergaya, F., Theng, B.G.K., Lagaly, G. (Eds.), Handbook of Clay Science. Elsevier, Amsterdam, pp. 1-18.

Bergaya F., Theng B.G.K. and Lagaly G. 2006 Handbook of Clay Science. Elsevier, Amsterdam.

Bickmore B.R., Rosso K.M., Nagy K.L., Cygan R.T. and Tadanier C.J. (2003) Ab initio determination of edge surface structures for dioctahedral 2 : 1 phyllosilicates: Implications for acid-base reactivity. *Clays and Clay Minerals* **51**: 359-371.

Bickmore B.R., Rosso K.M., Tadanier C.J., Bylaska E.J. and Doud D. (2006) Bond-valence methods for pK(a) prediction. II. Bond-valence, electrostatic, molecular geometry, and solvation effects. *Geochimica Et Cosmochimica Acta* **70**: 4057-4071.

Bish D.L. (1993) Rietveld refinement of the kaolinite structure at 1.5K. *Clays and Clay Minerals* **41**: 738-744.

Boek E.S. and Sprik M. (2003) Ab initio molecular dynamics study of the hydration of a sodium smectite clay. *J. Phys. Chem. B.* **107**: 3251-3256.

Boulet P., Greenwell H.C., Stackhouse S. and Coveney P.V. (2006) Recent advances in understanding the structure and reactivity of clays using electronic structure calculations. *Journal of Molecular Structure-Theochem* **762**: 33-48.

Bourg I.C., Sposito G. and Bourg A.C.M. (2007) Modeling the acid-base surface chemistry of montmorillonite. *Journal of Colloid and Interface Science* **312**: 297-310.

Bradbury M.H. and Baeyens B. (1997) A mechanistic description of Ni and Zn sorption on Na-montmorillonite .2. Modelling. *Journal of Contaminant Hydrology* **27**: 223-248.

Brady P.V., Cygan R.T. and Nagy K.L. (1996) Molecular controls on kaolinite surface charge. *Journal of Colloid and Interface Science* **183**: 356-364.

Charlet L., Schindler P.W., Spadini L., Furrer G. and Zysset M. (1993) Cation adsorption on oxides and clays - the aluminum case. *Aquatic Sciences* **55**: 291-303.

Cheng J. and Sprik M. (2010) Acidity of the Aqueous Rutile TiO2(110) Surface from Density Functional Theory Based Molecular Dynamics. *Journal of Chemical Theory and Computation* **6**: 880-889.

Cheng J., Sulpizi M. and Sprik M. (2009) Redox potentials and pK(a) for benzoquinone from density functional theory based molecular dynamics. *Journal of Chemical Physics* **131**.

Churakov S.V. (2006) Ab initio study of sorption on pyrophyllite: Structure and acidity of the edge sites. *Journal of Physical Chemistry B* **110**: 4135-4146.

Churakov S.V. (2007) Structure and dynamics of the water films confined between edges of pyrophyllite: A first principle study. *Geochimica Et Cosmochimica Acta* **71**: 1130-1144.

Churakov S.V. and Daehn R. (2012) Zinc Adsorption on Clays Inferred from Atomistic Simulations and EXAFS Spectroscopy. *Environmental Science & Technology* **46**: 5713-5719.
Churakov S.V. and Kosakowski G. (2010) An ab initio molecular dynamics study of hydronium complexation in Na-montmorillonite. *Philosophical Magazine* **90**: 2459-2474.
Churchman G.J., Gates W.P., Theng B.K.G. and Yuan G. 2006 Clays and clay minerals for pollution control. In: Bergaya, F., Theng, B.G.K., Lagaly, G. (Eds.), Handbook of Clay Science. Elsevier, Amsterdam, pp. 625-676.
Costanzo F., Sulpizi M., Della Valle R.G. and Sprik M. (2011) The oxidation of tyrosine and tryptophan studied by a molecular dynamics normal hydrogen electrode. *Journal of Chemical Physics* **134**.
Croteau T., Bertram A.K. and Patey G.N. (2009) Simulation of Water Adsorption on Kaolinite under Atmospheric Conditions. *Journal of Physical Chemistry A* **113**: 7826-7833.
Cygan R.T., Greathouse J.A., Heinz H. and Kalinichev A.G. (2009) Molecular models and simulations of layered materials. *Journal of Materials Chemistry* **19**: 2470-2481.
Cygan R.T., Liang J.-J. and Kalinichev A.G. (2004) Molecular Models of Hydroxide, Oxyhydroxide, and Clay Phases and the Development of a General Force Field. *Journal of Physical Chemistry B* **108**: 1255-1266.
Goedecker S., Teter M. and Hutter J. (1996) Separable dual-space Gaussian pseudopotentials. *Physical Review B* **54**: 1703-1710.
Gu X. and Evans L.J. (2008) Surface complexation modelling of Cd(II), Cu(II), Ni(II), Pb(II) and Zn(II) adsorption onto kaolinite. *Geochimica Et Cosmochimica Acta* **72**: 267-276.
Gu X., Evans L.J. and Barabash S.J. (2010) Modeling the adsorption of Cd (II), Cu (II), Ni (II), Pb (II) and Zn (II) onto montmorillonite. *Geochimica Et Cosmochimica Acta* **74**: 5718-5728.
Herdman G.J. and Neilson G.W. (1992) FERROUS FE(II) HYDRATION IN A 1-MOLAL HEAVY-WATER SOLUTION OF IRON CHLORIDE. *Journal of Physics-Condensed Matter* **4**: 649-653.
Ikhsan J., Johnson B.B. and Wells J.D. (1999) A comparative study of the adsorption of transition metals on kaolinite. *Journal of Colloid and Interface Science* **217**: 403-410.
Ikhsan J., Wells J.D., Johnson B.B. and Angove M.J. (2005) Surface complexation modeling of the sorption of Zn(II) by montmorillonite. *Colloids and Surfaces a-Physicochemical and Engineering Aspects* **252**: 33-41.
Kraepiel A.M.L., Keller K. and Morel F.M.M. (1999) A model for metal adsorption on montmorillonite. *Journal of Colloid and Interface Science* **210**: 43-54.
Lagaly G. 2006 Colloid clay science. In: Bergaya, F., Theng, B.G.K., Lagaly, G. (Eds.), Handbook of Clay Science. Elsevier, Amsterdam, pp. 141-246.
Lagaly G., Ogawa M. and Dekany I. 2006 Clay mineral organic interactions. In: Bergaya, F., Theng, B.G.K., Lagaly, G. (Eds.), Handbook of Clay Science. Elsevier, Amsterdam, pp. 309-377.
Laio A. and Parrinello M. (2002) Escaping free-energy minima. *Proceedings of the National Academy of Sciences of the United States of America* **99**: 12562-12566.
Larentzos J.P., Greathouse J.A. and Cygan R.T. (2007) An ab initio and classical molecular dynamics investigation of the structural and vibrational properties of talc and pyrophyllite. *J. Phys. Chem. C*. **111**: 12752–12759.
Lee C.T., Yang W.T. and Parr R.G. (1988) Development of the colle-salvetti correlation-energy formula into a functional of the electron-density. *Physical Review B* **37**: 785-789.
Lippert G., Hutter J. and Parrinello M. (1997) A hybrid Gaussian and plane wave density functional scheme. *Molecular Physics* **92**: 477-487.
Liu X.-D. and Lu X.-C. (2006) A thermodynamic understanding of clay-swelling inhibition by potassium ions. *Angewandte Chemie-International Edition* **45**: 6300-6303.
Liu X., Lu X., Meijer E.J., Wang R. and Zhou H. (2010) Acid dissociation mechanisms of Si(OH)(4) and Al(H2O)(6)(3+) in aqueous solution. *Geochimica Et Cosmochimica Acta* **74**: 510-516.
Liu X., Lu X., Meijer E.J., Wang R. and Zhou H. (2012a) Atomic-scale structures of interfaces between phyllosilicate edges and water. *Geochimica Et Cosmochimica Acta* **81**: 56-68.

Liu X., Lu X., Wang R., Meijer E.J. and Zhou H. (2011) Acidities of confined water in interlayer space of clay minerals. *Geochimica Et Cosmochimica Acta* **75**: 4978-4986.

Liu X., Lu X., Wang R., Meijer E.J., Zhou H. and He H. (2012b) Atomic-scale structures of interfaces between kaolinite edges and water. *Geochimica Et Cosmochimica Acta* **92**: 233-242.

Liu X., Meijer E.J., Lu X. and Wang R. (2012c) FIRST-PRINCIPLES MOLECULAR DYNAMICS INSIGHT INTO Fe2+ COMPLEXES ADSORBED ON EDGE SURFACES OF CLAY MINERALS. *Clays and Clay Minerals* **60**: 341-347.

Mangold M., Rolland L., Costanzo F., Sprik M., Sulpizi M. and Blumberger J. (2011) Absolute pK(a) Values and Solvation Structure of Amino Acids from Density Functional Based Molecular Dynamics Simulation. *Journal of Chemical Theory and Computation* **7**: 1951-1961.

Marcussen H., Holm P.E., Strobel B.W. and Hansen H.C.B. (2009) Nickel Sorption to Goethite and Montmorillonite in Presence of Citrate. *Environmental Science & Technology* **43**: 1122-1127.

Marx D. and Hutter J., 2009. Ab Initio Molecular Dynamics: Basic Theory and Advanced Methods Cambridge University Press, Cambridge.

Ockwig N.W., Greathouse J.A., Durkin J.S., Cygan R.T., Daemen L.L. and Nenoff T.M. (2009) Nanoconfined Water in Magnesium-Rich 2:1 Phyllosilicates. *Journal of the American Chemical Society* **131**: 8155-8162.

Rotenberg B., Marry V., Vuilleumier R., Malikova N., Simon C. and Turq P. (2007) Water and ions in clays: Unraveling the interlayer/micropore exchange using molecular dynamics. *Geochimica Et Cosmochimica Acta* **71**: 5089-5101.

Schindler P.W., Liechti P. and Westall J.C. (1987) Adsorption of copper, cadmium and lead from aqueous-solution to the kaolinite water interface. *Netherlands Journal of Agricultural Science* **35**: 219-230.

Schoonheydt R.A. and Johnston C.T. 2006 Surface and interface chemistry of clay minerals. In: Bergaya, F., Theng, B.G.K., Lagaly, G. (Eds.), Handbook of Clay Science. Elsevier, Amsterdam, pp. 87-112.

Schultz C. and Grundl T. (2004) pH dependence of ferrous sorption onto two smectite clays. *Chemosphere* **57**: 1301-1306.

Skelton A.A., Fenter P., Kubicki J.D., Wesolowski D.J. and Cummings P.T. (2011) Simulations of the Quartz(10(1)over-bar1)/Water Interface: A Comparison of Classical Force Fields, Ab Initio Molecular Dynamics, and X-ray Reflectivity Experiments. *Journal of Physical Chemistry C* **115**: 2076-2088.

Sposito G. 1984 The Surface Chemistry of Soils. Oxford Univ. Press, New York.

Sprik M. (2000) Computation of the pK of liquid water using coordination constraints. *Chemical Physics* **258**: 139-150.

Sprik M. and Ciccotti G. (1998) Free energy from constrained molecular dynamics. *Journal of Chemical Physics* **109**: 7737-7744.

Srivastava P., Singh B. and Angove M. (2005) Competitive adsorption behavior of heavy metals on kaolinite. *Journal of Colloid and Interface Science* **290**: 28-38.

Sulpizi M., Gaigeot M.-P. and Sprik M. (2012) The Silica-Water Interface: How the Silanols Determine the Surface Acidity and Modulate the Water Properties. *Journal of Chemical Theory and Computation* **8**: 1037-1047.

Sulpizi M. and Sprik M. (2008) Acidity constants from vertical energy gaps: density functional theory based molecular dynamics implementation. *Physical Chemistry Chemical Physics* **10**: 5238-5249.

Sulpizi M. and Sprik M. (2010) Acidity constants from DFT-based molecular dynamics simulations. *Journal of Physics-Condensed Matter* **22**.

Suter J.L., Anderson R.L., Greenwell H.C. and Coveney P.V. (2009) Recent advances in large-scale atomistic and coarse-grained molecular dynamics simulation of clay minerals. *Journal of Materials Chemistry* **19**: 2482-2493.

Suter J.L., Boek E.S. and Sprik M. (2008) Adsorption of a Sodium Ion on a Smectite Clay from Constrained Ab Initio Molecular Dynamics Simulations. *Journal of Physical Chemistry C* **112**: 18832-18839.

Tazi S., Benjamin Rotenberg, Mathieu Salanne, Michiel Sprik and Sulpizi M. (2012) Absolute acidity of clay edge sites from ab-initio simulations. *Geochimica Et Cosmochimica Acta* **94**: 1-11.

Tertre E., Castet S., Berger G., Loubet M. and Giffaut E. (2006) Surface chemistry of kaolinite and Na-montmorillonite in aqueous electrolyte solutions at 25 and 60 degrees C: Experimental and modeling study. *Geochimica Et Cosmochimica Acta* **70**: 4579-4599.

Tombacz E., Nyilas T., Libor Z. and Csanaki C. 2004 Surface charge heterogeneity and aggregation of clay lamellae in aqueous suspensions. In: Zrinyi, M.H.Z.D. (Ed.), From Colloids to Nanotechnology. Progress in Colloid and Polymer Science, pp. 206-215.

Tombacz E. and Szekeres M. (2004) Colloidal behavior of aqueous montmorillonite suspensions: the specific role of pH in the presence of indifferent electrolytes. *Applied Clay Science* **27**: 75-94.

Tournassat C., Ferrage E., Poinsignon C. and Charlet L. (2004) The titration of clay minerals II. Structure-based model and implications for clay reactivity. *Journal of Colloid and Interface Science* **273**: 234-246.

Tunega D., Benco L., Haberhauer G., Gerzabek M.H. and Lischka H. (2002a) Ab initio molecular dynamics study of adsorption sites on the (001) surfaces of 1 : 1 dioctahedral clay minerals. *Journal of Physical Chemistry B* **106**: 11515-11525.

Tunega D., Gerzabek M.H. and Lischka H. (2004) Ab initio molecular dynamics study of a monomolecular water layer on octahedral and tetrahedral kaolinite surfaces. *Journal of Physical Chemistry B* **108**: 5930-5936.

Tunega D., Gerzabek M.H. and Totsche K.U. (2011) Advances of molecular modeling of biogeochemical interfaces in soils. *Geoderma* **169**: 1-3.

Tunega D., Haberhauer G., Gerzabek M.H. and Lischka H. (2002b) Theoretical study of adsorption sites on the (001) surfaces of 1 : 1 clay minerals. *Langmuir* **18**: 139-147.

VandeVondele J., Krack M., Mohamed F., Parrinello M., Chassaing T. and Hutter J. (2005a) QUICKSTEP: Fast and accurate density functional calculations using a mixed Gaussian and plane waves approach. *Computer Physics Communications* **167**: 103-128.

VandeVondele J., Mohamed F., Krack M., Hutter J., Sprik M. and Parrinello M. (2005b) The influence of temperature and density functional models in ab initio molecular dynamics simulation of liquid water. *Journal of Chemical Physics* **122**.

Vasconcelos I.F., Bunker B.A. and Cygan R.T. (2007) Molecular dynamics modeling of ion adsorption to the basal surfaces of kaolinite. *Journal of Physical Chemistry C* **111**: 6753-6762.

Viani A., Gaultieri A.F. and Artioli G. (2002) The nature of disorder in montmorillonite by simulation of X-ray powder patterns. *American Mineralogist* **87**: 966-975.

Wanner H., Albinsson Y., Karnland O., Wieland E., Wersin P. and Charlet L. (1994) The acid-base chemistry of montmorillonite. *Radiochimica Acta* **66-7**: 157-162.

Westermann K., Naser K.-H. and Brandes G. 1986 InorganicChemistry (Anorganische Chemie). VEB Deutscher Verlag fiir Grundstoffindustrie, Leipzig, GDR.

Zachara J.M. and Smith S.C. (1994) Edge complexation reactions of cadmium on specimen and soil-derived smectite. *Soil Science Society of America Journal* **58**: 762-769.